Rectification of radio-frequency current in a giant-magnetoresistance spin valve

Sławomir Ziętek,[1,*] Piotr Ogrodnik,[1,2,†] Marek Frankowski,[1,‡] Jakub Chęciński,[1,3] Piotr Wiśniowski,[1] Witold Skowroński,[1] Jerzy Wrona,[1,4] Tomasz Stobiecki,[1] Antoni Żywczak,[5] and Józef Barnaś[6,7]

[1]*Department of Electronics, AGH University of Science and Technology, Aleja Mickiewicza 30, 30-059 Kraków, Poland*

[2]*Faculty of Physics, Warsaw University of Technology, Ulica Koszykowa 75, 00-662 Warszawa, Poland*

[3]*Faculty of Physics and Applied Computer Science, AGH University of Science and Technology, Aleja Mickiewicza 30, 30-059 Kraków, Poland*

[4]*Singulus Technologies, 63796 Kahl am Main, Germany*

[5]*Academic Centre of Materials and Nanotechnology, AGH University of Science and Technology, Aleja Mickiewicza 30, 30-059 Kraków, Poland*

[6]*Faculty of Physics, Adam Mickiewicz University, Ulica Umultowska 85, 61-614 Poznań, Poland*

[7]*Institute of Molecular Physics, Polish Academy of Sciences, Ulica Smoluchowskiego 17, 60-179 Poznań, Poland*

(Received 27 October 2014; published 26 January 2015)

We report on a highly efficient spin diode effect in exchange-biased spin-valve giant-magnetoresistance (GMR) strips. In such multilayer structures, the symmetry of the current distribution along the vertical direction is broken and, as a result, a noncompensated Oersted field acting on the magnetic free layer appears. This field in turn is a driving force of magnetization precessions. Due to the GMR effect, the resistance of the strip oscillates following the magnetization dynamics. This leads to rectification of the applied radio-frequency current and induces a direct-current voltage V_{dc}. We present a theoretical description of this phenomenon and calculate the spin diode signal V_{dc} as a function of frequency, external magnetic field, and angle at which the external field is applied. Satisfactory quantitative agreement between theoretical predictions and experimental data has been achieved. Finally, we show that the spin diode signal in GMR devices is significantly stronger than in the anisotropic magnetoresistance permalloy-based devices.

DOI: 10.1103/PhysRevB.91.014430 PACS number(s): 76.50.+g, 75.78.−n, 75.47.De

I. INTRODUCTION

Radio-frequency (rf) devices have been of significant interest for a long time due to their multiple applications, e.g., in wireless telecommunication, fast electronics, or radar technologies. Due to certain limitations of the semiconductor technology, new materials and phenomena that could be applied in microwave devices are highly desired [1,2]. Ferromagnetic resonance (FMR) in magnetic multilayer systems, which is typically probed in the rf regime, gives a chance to create new microwave nanodevices such as filters, rectifiers, oscillators, phase shifters, or delay lines [1,3].

An ac current passing through a magnetic structure can entail an oscillation of the magnetization due to the spin transfer torque, field torque, or spin-orbit torque [4–7]. This oscillation in turn results in the variation of the resistance due to the magnetoresistance effect. The oscillating resistance mixed with the ac current gives rise to a dc voltage component and this rectification is called a spin diode effect [8], which has been widely investigated in nanostructured magnetic tunnel junctions (MTJs) [8–13] as well as in different thin-film systems based on Py [4,14–16], Fe [17], and other materials and compounds [7,18–28].

Extensive theoretical research has been carried out in order to examine the physical foundations of the phenomena involved in rf devices [4–6]. It has been shown that a proper analysis of the FMR-generated dc voltage requires distinguishing between different mechanisms contributing to the symmetrical and antisymmetrical components of the signal [5]. The role of the relative phase difference between rf electric and magnetic fields has also been discussed in literature, as summarized by Harder *et al.* in Ref. [5]. Although experimental data reported by several groups are consistent, there are some discrepancies in theoretical descriptions of the physical origin of the dc voltage V_{dc}.

Most of the recent studies on the spin diode effect focused either on devices exhibiting the anisotropic magnetoresistance (AMR) effect or on MTJs with tunneling magnetoresistance. The spin diode signal in AMR devices is usually very weak due to a low-magnetoresistance ratio. In MTJs, on the other hand, a much stronger diode signal is usually observed. Operation of the MTJ-based devices, however, is limited to voltages below the corresponding breakdown values. In this paper we report on a spin diode effect in an exchange-biased spin-valve giant-magnetoresistance (SVGMR) strip, which is an alternative to AMR- or MTJ-based devices. Very recently, a similar SVGMR strip was investigated by Kleinlein *et al.* [29]. The authors, however, focused their attention mainly on its enhanced detection sensitivity when compared to an AMR-based device.

In Sec. II we provide a theoretical description of the dc voltage and the electrically detected FMR spectra. In Sec. III we describe the preparation process of the investigated multilayer strip, the experimental setup used to detect a spin diode signal, and the origin of the Oersted field affecting the free-layer dynamics. Results obtained, including the angular and frequency dependences of the signal, are presented in Sec. IV, where we also discuss the nature of the magnetization oscillations responsible for time-dependent resistance changes as well as the physical origin of the dc voltage signal. The experimental data are compared with theoretical predictions

*zietek@agh.edu.pl
†piotrogr@if.pw.edu.pl
‡mfrankow@agh.edu.pl

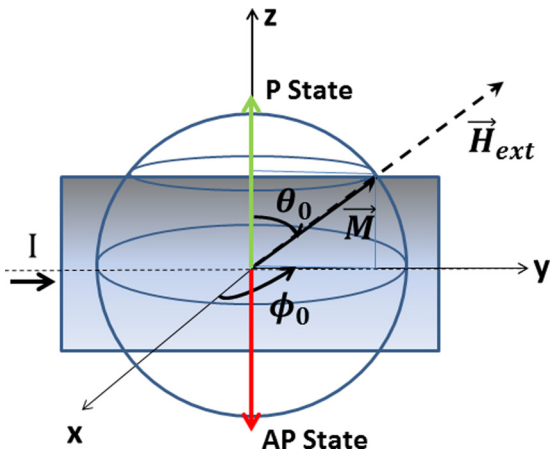

FIG. 1. (Color online) Top view of the SVGMR structure under consideration: Magnetization of the RL is oriented along the axis z, while that of the FL is oriented along the external in-plane y-z magnetic field direction. The polar θ_0 and azimuthal ϕ_0 angles, which determine orientation of the FL magnetization in the equilibrium situation, are also indicated. The parallel (P) state corresponds to $\theta_0 = 0$ and the antiparallel (AP) configuration to $\theta_0 = \pi$. The ac current flowing through the structure is oriented along the axis y. Magnetization is aligned along the external field direction since the uniaxial anisotropy field in our experiment is negligibly small (see Sec. III A).

for the angular and frequency dependences of the spin diode signal. Finally, Sec. V contains a short summary and conclusions.

II. THEORY

A. General background on V_{dc}

In this section we present some general theoretical background on the spin diode effect, based on the description by Nozaki *et al.* [30] for magnetoresistive tunnel junctions. This description is then adapted to the experimental SVGMR system. For this purpose, we define a coordinate system with respect to the sample orientation, as presented in Fig. 1. Consecutive layers of the structure lie in the y-z plane and we assume that the magnetization of the reference layer (RL) is pinned along the z axis and does not affect the dynamics of the free layer (FL). The polar angle θ is defined as the angle between the magnetization $\vec{M}$ of the FL and the magnetization of the RL. This angle also determines the resistance of the SVGMR according to the formula

$$R(\theta) = R_P + \frac{\Delta R}{2}(1 - \cos\theta), \tag{1}$$

where $\Delta R = R_{AP} - R_P$, while R_P and R_{AP} denote resistances in the parallel and antiparallel states, respectively.

A well-established fact is that the application of a radio-frequency voltage $V(t) = V\cos(\omega t) = \mathcal{R}\{Ve^{i\omega t}\}$ to a magnetoresistive strip generates a time-dependent driving force (due to spin torque [4,10], Oersted field [31], or anisotropy field [30]) that may generate oscillations of the magnetization of the FL. These oscillations result in small changes of the resistance $\delta R(t) = \delta\bar{R}\cos(\omega t + \beta) = \mathcal{R}\{\delta\bar{R}e^{i(\omega t+\beta)}\}$. Here β is a phase shift between the time-dependent current and the resistance, while $\delta\bar{R}$ is the amplitude (real) of the resistance change. Since the ac current flowing through the sample depends mainly on the resistance in the corresponding stationary point described by θ_0 and ϕ_0, it can be approximated by $I(t) = \frac{V\cos(\omega t)}{R(\theta_0)}$ and thus the applied ac voltage and ac current are in phase. Note that the stationary point is determined by the magnetic energy in the absence of the ac signal.

The output dc voltage V_{dc} is determined by the product of the time-dependent resistance and the current. Apart from the dc voltage, this product also includes the ac voltage V_{ac} of doubled frequency. Thus, we can write [30]

$$V_{out} = V_{dc} + V_{ac} = \frac{1}{R(\theta_0)}\mathcal{R}\{Ve^{i\omega t}\}\mathcal{R}\{\delta\bar{R}e^{i(\omega t+\beta)}\}. \tag{2}$$

From this equation one easily finds

$$V_{dc} = \frac{V}{2}\frac{\delta\bar{R}}{R(\theta_0)}\cos\beta. \tag{3}$$

The voltage V_{dc} can be detected, for instance, in a FMR dynamics experiment [30]. The point is that the phase shift β and the amplitude of the resistance change $\delta\bar{R}$ are not constant, but generally depend on the frequency. Therefore, the simple formula (3) for V_{dc} is rather useless for interpretation of experimental data and one needs to derive a more general expression for V_{dc}. To do this, we rewrite the expression for V_{dc} in the form in which the phase shift is not extracted explicitly, but is included in the resistance change $\delta\bar{R}e^{i\beta} \equiv \delta R$,

$$V_{dc} = \eta\frac{V}{2}\frac{\mathcal{R}\{\delta R\}}{R(\theta_0)}, \tag{4}$$

where we introduced an additional phenomenological factor η that originates from both parasitic impedances of the measurement setup and the impedance of the sample. The parameter η will be treated as a free parameter and will allow us to compare the experimental and theoretical results quantitatively [30]. It is important to note that η influences neither the shape of the resonance spectra nor their linewidths and the resonant frequencies, but instead acts rather as a scaling factor that modifies only the absolute values of the spectrum amplitude.

To determine the V_{dc} signal, one needs to determine the resistance change δR in Eq. (4) around the stationary point θ_0 for a given ac voltage. Thus, using Eq. (1) and calculating the first derivative at θ_0, one finds

$$\delta R = \frac{\Delta R}{2}\sin(\theta_0)\delta\theta, \tag{5}$$

where $\delta\theta$ is a change in the polar angle due to the magnetization dynamics. Combining this with Eq. (4) allows us to write the dc voltage signal in the form

$$V_{dc} = \eta\frac{V}{4}\frac{\Delta R}{R(\theta_0)}\sin(\theta_0)\mathcal{R}\{\delta\theta\}. \tag{6}$$

What we need now is to calculate the angle change $\delta\theta$ that can be derived from the Landau-Lifshitz-Gilbert (LLG) equation.

B. The FMR resonance theory of V_{dc}

To calculate $\delta\theta$ we use the LLG equation in the macrospin approximation

$$\frac{d\vec{M}}{dt} = -\gamma_e \vec{M} \times \vec{H}_{\text{eff}} + \frac{\alpha}{M_S}\vec{M} \times \frac{d\vec{M}}{dt}, \tag{7}$$

where $\gamma_e = \frac{g\mu_B}{\hbar}$ is the gyromagnetic ratio with the spectroscopic splitting factor $g = 2.1$ ($\gamma_e > 0$), M_S denotes the saturation magnetization of the FL, $\vec{H}_{\text{eff}}$ stands for the effective magnetic field, which can be described by the corresponding magnetic energy density U, $\vec{H}_{\text{eff}} = -\partial U/\partial \vec{M}$. In the SVGMR structure under consideration, the driving force for FMR originates from the time-dependent Oersted field associated with the ac current flowing along the strip. This assumption will be discussed in more detail in the next section, where it will be shown that it is sufficient to describe experimental results. Generally, the Oersted field cannot be written as a gradient of a potential energy due to its rotational character $\vec{\nabla} \times \vec{H}_{\text{Oe}} \neq 0$ [32]. In our case, however, we take into account the Oersted field only in the FL. This field is uniform and oriented along the z axis $\vec{H}_{\text{Oe},z} \equiv H_{\text{Oe}}$, so the associated energy is simply the Zeeman energy that can be included in U.

By introducing unit vectors $\hat{e}_\theta$ and $\hat{e}_\phi$ associated with the spherical coordinates [33], one can rewrite the LLG equation (7) as the following differential equation:

$$\begin{aligned}&[\sin(\theta)\dot{\phi}\hat{e}_\phi + \dot{\theta}\hat{e}_\theta] + \alpha\sin(\theta)\dot{\phi}\hat{e}_\phi - \alpha\dot{\theta}\hat{e}_\phi \\ &= \frac{\gamma_e}{M_S}\frac{\partial U}{\partial\theta}\hat{e}_\phi - \frac{\gamma_e}{M_S\sin\theta}\frac{\partial U}{\partial\phi}\hat{e}_\theta.\end{aligned} \tag{8}$$

Since the magnetization of the FL is driven by a periodic Oersted field, one can assume that both spherical angles oscillate periodically with small amplitudes around the stationary point (θ_0,ϕ_0): $\theta(t) = \theta_0 + \delta\theta e^{i\omega t}$ and $\phi(t) = \phi_0 + \delta\phi e^{i\omega t}$. Note that $\delta\theta$ and $\delta\phi$ include a possible phase shift between the magnetization oscillation and the driving ac current. Equation (8) can then be rewritten as two coupled equations for $\delta\theta$ and $\delta\phi$,

$$\begin{pmatrix} i\omega\delta\theta \\ i\omega\delta\phi \end{pmatrix} = \begin{pmatrix} \frac{1}{M_S}\frac{-\gamma_e}{1+\alpha^2}\left(\frac{1}{\sin\theta}\frac{\partial U}{\partial\phi} + \alpha\frac{\partial U}{\partial\theta}\right) \\ \frac{1}{M_S}\frac{-\gamma_e}{1+\alpha^2}\left(-\frac{1}{\sin\theta}\frac{\partial U}{\partial\theta} + \frac{\alpha}{\sin^2\theta}\frac{\partial U}{\partial\phi}\right) \end{pmatrix}. \tag{9}$$

Upon linearization with respect to small deviations $\delta\theta$ and $\delta\phi$ from the stationary point (θ_0,ϕ_0), the LLG equation (9) takes the form

$$\begin{pmatrix} \left[i\omega(1+\alpha^2) + \frac{\gamma_e}{\sin\theta}B + \frac{\cos\theta}{\sin^2\theta}A + \alpha\gamma_e D\right] & \gamma_e\left(\frac{1}{\sin\theta}C + \alpha B\right) \\ \gamma_e\left(\frac{\cos\theta}{\sin^2\theta}E - \frac{1}{\sin\theta}D - 2\frac{\alpha\cos\theta}{\sin^3\theta}A + \frac{\alpha}{\sin^2\theta}B\right) & \left[i\omega(1+\alpha^2) - \gamma_e\left(B\frac{1}{\sin\theta} - \alpha C\frac{1}{\sin^2\theta}\right)\right] \end{pmatrix}\begin{pmatrix}\delta\theta \\ \delta\phi\end{pmatrix} = \begin{pmatrix} -\gamma_e\left(H\frac{1}{\sin\theta} + \alpha M\right) \\ \gamma_e\left(\frac{1}{\sin\theta}M - \alpha H\frac{1}{\sin^2\theta}\right)\end{pmatrix} H_{\text{Oe}}e^{i\psi}, \tag{10}$$

where we have introduced parameters denoting first and second derivatives of the magnetic energy: $A \equiv \frac{1}{M_S}\frac{\partial U}{\partial\phi}$, $B \equiv \frac{1}{M_S}\frac{\partial^2 U}{\partial\phi\partial\theta}$, $C \equiv \frac{1}{M_S}\frac{\partial^2 U}{\partial\phi^2}$, $D \equiv \frac{1}{M_S}\frac{\partial^2 U}{\partial\theta^2}$, $E \equiv \frac{1}{M_S}\frac{\partial U}{\partial\theta}$, $H \equiv \frac{1}{M_S}\frac{\partial^2 U}{\partial\phi\partial H_{\text{Oe}}}$, and $M \equiv \frac{1}{M_S}\frac{\partial^2 U}{\partial\theta\partial H_{Oe}}$. The introduced phase factor ψ stands for the phase shift between the electric and the magnetic fields (or equivalently between the ac current and the ac Oersted field) [5].

Equation (10) has the general form $\hat{A}\hat{X} = \hat{Y}$, where $\hat{A}$ denotes the matrix on the left-hand side of Eq. (10), $\hat{X}$ is the vector composed of $\delta\theta$ and $\delta\phi$, and $\hat{Y}$ is the right-hand side of Eq. (10). This equation can be solved by multiplying both sides by the inverse matrix $\hat{A}^{-1}$. After some algebra, one finds $\hat{A}^{-1}$ in the explicit form

$$\hat{A}^{-1} = \frac{-1}{\Gamma(\omega^2 - \omega_0^2 - i\omega\sigma)}\begin{pmatrix} i(1+\alpha^2)\omega + \frac{-\gamma_e}{\sin\theta}\left(B - C\frac{\alpha}{\sin\theta}\right) & \gamma_e\left(-B\alpha - C\frac{1}{\sin\theta}\right) \\ \frac{\gamma_e}{\sin\theta}\left(D - E\frac{\cos\theta}{\sin\theta} - B\frac{\alpha}{\sin\theta} + 2A\alpha\frac{\cos\theta}{\sin^2\theta}\right) & i(1+\alpha^2)\omega - \gamma_e\left(A\frac{\cos\theta}{\sin^2\theta} - D\alpha - B\frac{1}{\sin\theta}\right). \end{pmatrix}. \tag{11}$$

In this equation Γ is defined as $\Gamma \equiv (1+\alpha^2)^2$, while the square of the angular resonance frequency and the corresponding linewidth are given respectively by the following formulas:

$$\omega_0^2 \equiv \frac{\gamma_e^2}{\Gamma}\frac{1}{\sin\theta}\left[\frac{1+\alpha^2}{\sin\theta}(CD - B^2) + \frac{\cos\theta}{\sin\theta}\left(-EB\alpha + \frac{1}{\sin\theta}(2\alpha^2 AB + AB - EC) + \frac{\alpha}{\sin^2\theta}AC\right)\right] \tag{12}$$

and

$$\sigma \equiv \frac{\gamma_e}{(1+\alpha^2)}\left[\alpha D - \frac{\cos\theta}{\sin^2\theta}A + \frac{\alpha}{\sin^2\theta}C\right]. \tag{13}$$

Taking into account Eqs. (10) and (11), one can easily find the solutions for $\delta\theta$ and $\delta\phi$. Then the real part of the solution for $\delta\theta$ can be introduced into Eq. (4), which leads to the final result for the V_{dc} signal originating from the Oersted field for an arbitrary form of the magnetic energy:

$$V_{\text{dc}} = \eta\frac{I H_{\text{Oe}}\Delta R\sin\theta}{4}\frac{\gamma_e}{\Gamma^{1/2}[(\omega^2 - \omega_0^2)^2 + \omega^2\sigma^2]}[\cos(\psi)Z_1 - \sin(\psi)Z_2], \tag{14}$$

where

$$Z_1 = -\sigma\omega^2(M\alpha + H\csc\theta) - \gamma_e\csc^2(\theta)\left(\omega^2 - \omega_0^2\right)(BH - CM), \tag{15}$$

$$Z_2 = \omega\left(\omega^2 - \omega_0^2\right)(M\alpha + H\csc\theta) - \gamma_e\csc^2(\theta)\sigma\omega(BH - CM), \tag{16}$$

and I denotes the amplitude of the ac current flowing through the sample at a given angle θ_0. The phase shift ψ has a significant influence on the shape of the FMR spectra and, for a given form of energy U, may change their character from antisymmetrical to symmetrical and vice versa.

To complete this section, we note that the factor $[\cos(\psi)Z_1 - \sin(\psi)Z_2]$ in Eq. (14) can be written in a form consistent with Eq. (3). Writing Z_1 and Z_2 as $Z_1/(Z_1^2 + Z_2^2) = \cos\Phi$ and $Z_2/(Z_1^2 + Z_2^2) = \sin\Phi$, one can rewrite this factor in the form

$$\begin{aligned}&[\cos(\psi)Z_1 - \sin(\psi)Z_2]\\ &= \left(Z_1^2 + Z_2^2\right)[\cos\psi\cos\Phi - \sin\psi\sin\Phi]\\ &= \left(Z_1^2 + Z_2^2\right)\cos(\psi + \Phi),\end{aligned}$$

i.e., in the form (3) with β ($\beta = \psi + \Phi$) and the prefactor explicitly dependent on the frequency and other parameters of the model.

III. EXPERIMENT

A. The SVGMR device: Fabrication

The material stack with the structure (nominal thicknesses in nm) $Si/SiO_2/Ta(3)/Ni_{81}Fe_{19}(1)/Pt_{46}Mn_{54}(18)/Co_{90}Fe_{10}(2)/Ru(0.85)/Co_{90}Fe_{10}(2.1)/Cu(2.1)/Co_{90}Fe_{10}(1)/Ni_{81}Fe_{19}(5)/Ru(0.5)/Cu(1)/Ta(3)$ was deposited by the TIMARIS magnetron sputtering system at Singulus AG. The easy axis of the magnetic layers was set by applying a 100-Oe field during layer deposition. The Cu thickness (2.1 nm) was chosen to minimize the interlayer coupling between the FL and RL. A CoFe/NiFe composite was used to achieve a magnetically soft FL with large magnetoresistance sustained by the Cu/CoFe interface [34,35]. Before the microfabrication process, the wafer was annealed in high vacuum at 280 °C for 1 h in a magnetic field of 5 kOe. The GMR strips with short and long axes of 2.5 and 70 μm were patterned using direct write laser lithography and ion beam milling. The wafer was patterned so that the easy axis of the magnetic free and reference layers were oriented along the shorter length of strips. In order to determine magnetizations, anisotropies, and interlayer exchange coupling energies of the multilayer stack, we performed measurements using a vibrating sample magnetometer (VSM). From the magnetization hysteresis loop in a high magnetic field we determined the saturation magnetization of the FL to be 1.03 T, the saturation magnetization of the RL to be 1.65 T, and the exchange bias energy to be 0.32 mJ/m^2. The uniaxial anisotropy energy of 0.8 kJ/m^3 was determined from the low magnetic field hysteresis loop.

B. Origin of the Oersted field

In order to investigate the magnetization dynamics induced by the Oersted field we have performed micromagnetic simulations for a homogeneous ferromagnetic strip using an object-oriented micromagnetic framework [36]. We have found that if the current distribution in the single layer strip is uniform, the FMR modes excited by alternating Oersted fields do not contribute to the measured signal when averaged over the whole sample. In order to obtain a rectification signal, a noncompensated Oersted field component originating from some kind of symmetry breaking is needed. This conclusion is in agreement with previous investigations [31], where mechanisms such as layer thickness effects described by the Sondheimer-Fuchs model [37] and contact region influence were proposed to explain the origin of a nonzero resultant field. However, in the case of the SVGMR strip we used, the asymmetry of the structure itself is sufficient to obtain a noncompensated Oersted field component. In order to calculate the magnitude of the resultant field, we have used the estimations for thin-film resistivities of the materials based on Refs. [38–42]. We have obtained resistance and current proportions for each layer, treating all layers as resistors connected in parallel, as depicted in Fig. 2. We have assumed that the current distribution is homogeneous within each layer. The total ac amplitude has been taken from the experimental data. The resultant current distribution has been integrated over the whole sample using the Biot-Savart law in order to obtain the Oersted field distribution. As shown in Fig. 2, the total field in the free layer consists of several components originating from different layers, resulting in an uncompensated Oersted field with an amplitude of 21.23 Oe, which is sufficiently large to enable the FL magnetization coherent precession and the observed diode effect. Since it is only the resultant component of the Oersted field that induces the measured effect and the external field of 100 Oe generated by Helmholtz coils used in the experiment is strong enough to saturate the FL, we conclude that the macrospin approach is suitable for theoretical analysis.

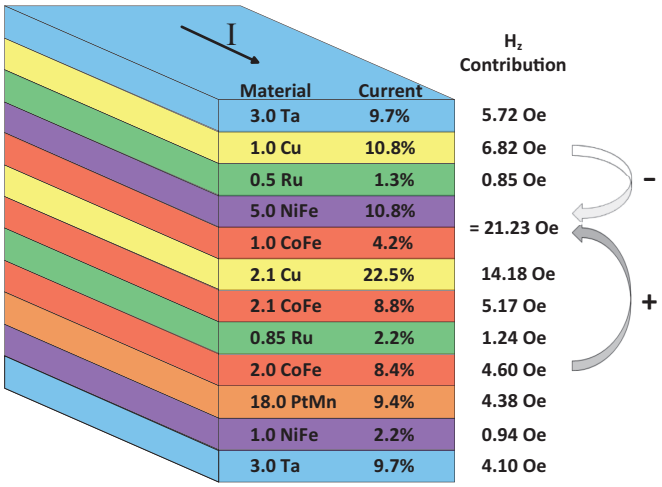

FIG. 2. (Color online) Current distribution in the GMR stack and magnetic field contribution from each layer. Note that the Oersted field contribution from the Cu spacer layer is dominant.

C. Experimental setup

The measurement setup consisted of a rf generator, a voltmeter, two pairs of Helmholtz coils oriented perpendicular to each other, and a bias tee to separate the dc voltage component from the rf voltage (Fig. 3). We applied a microwave signal of 10 dBm from the generator to the strip via the ground-signal rf probe and the dc voltage originating from the spin diode effect [8] was measured using magnetic field sweep along a

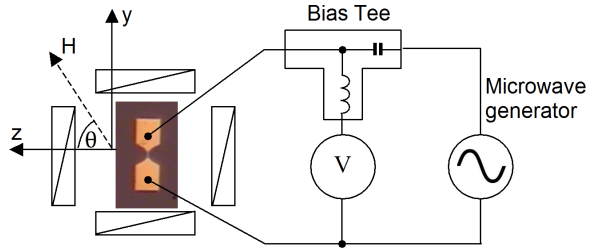

FIG. 3. (Color online) Schematic of the experimental setup for the spin diode effect detection. The axis z denotes the exchange bias direction.

given direction or the rotation of the magnetic field of constant magnitude within the y-z plane. The angle θ between the magnetic field (or magnetization of the FL) and the z axis was varied by rotating the magnetic field. The GMR measured in the strip was equal to 7.4%. Due to an impedance mismatch, the rf reflection coefficient was $\gamma = \frac{R-Z_0}{R+Z_0} = 0.537$, where $Z_0 = 50\ \Omega$ is the impedance of the measurement system used. As a result, only $1-\gamma^2 = 71\%$ of the initial microwave power of 10 mW (10 dBm) applied to the strip was actually absorbed, leading to the maximum current $I_{\rm rf} = 6.5$ mA.

IV. RESULTS AND DISCUSSION

A. Effective field

In order to analyze the FMR dynamics and compare the experimental results with theoretical predictions, one needs to know the explicit form of the effective magnetic field $\vec{H}_{\rm eff}$ within the sample. Based on experimental evidence, we can write the magnetic energy density in the form

$$U = K_{\parallel}\sin^2\theta - M_S \times\left(\vec{H}_{\rm ext}\cdot\hat{e}_M - \frac{M_S}{2\mu_0}\hat{e}_M^T\hat{N}\hat{e}_M + H_{\rm Oe}\hat{e}_z\cdot\hat{e}_M\right), \quad (17)$$

where $\hat{e}_M$ is a unit vector along the magnetization of the FL, $\hat{N}$ is demagnetization tensor in a standard form, $K_{\parallel}$ describes the in-plane uniaxial magnetic anisotropy, and $H_{\rm Oe}$ is the amplitude of the uncompensated Oersted field in the z direction. This form of the magnetostatic energy allows us to calculate derivatives in Eqs. (12)–(14) at a given stationary angle θ_0 set up by the external magnetic field. In particular, we are interested in the resonance frequency ($f_0 = \omega_0/2\pi$) for $\theta = 90^\circ$, at which the measured $V_{\rm dc}$ signal is the strongest one:

$$f_0 = \frac{\omega_0}{2\pi} = \frac{\gamma_e}{2\pi}\left\{\Gamma^{3/2}\left[H_{\rm ext} + \frac{M_S}{\mu_0}(N_x - N_y)\right] \times\left(-H_{K_{\parallel}} + H_{\rm ext} + \frac{M_S}{\mu_0}(N_z - N_y)\right)\right\}^{1/2}, \quad (18)$$

where we expressed the uniaxial anisotropy in terms of the anisotropy field $H_{K_{\parallel}} = 2K_{\parallel}/M_S$. Because of experimental conditions, we can neglect the symmetrical (antisymmetrical) contribution to Z_1 (Z_2), which is much smaller than its corresponding antisymmetrical (symmetrical) counterpart for $\psi = 0$, and thus rewrite Z_1 (Z_2) from Eq. (14) for $\phi = \pi/2$ as

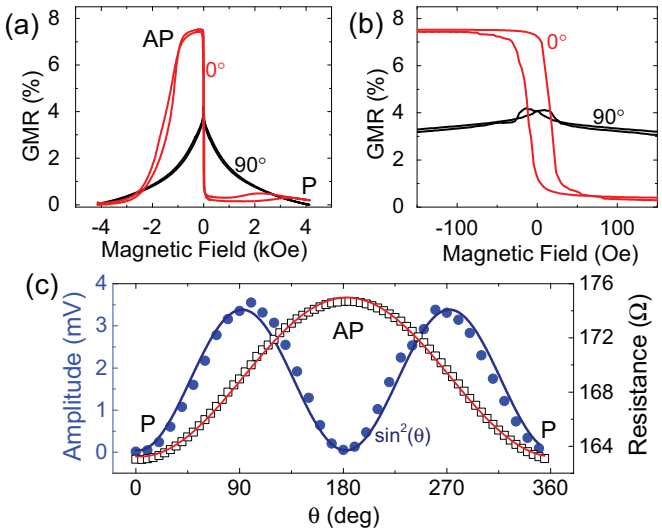

FIG. 4. (Color online) The GMR loops measured in (a) a wide magnetic field range and (b) a small magnetic field range. (c) Angular dependence of the resistance measured in 100 Oe (black open squares), theoretical curve based on Eq. (1) (red solid line), spin diode dc voltage (blue closed circles), and theoretical curve based on Eq. (21) (blue solid line).

$$Z_1 \approx \gamma_e\csc\theta\left(H_{\rm ext}\sin^2\theta + \frac{M_S}{\mu_0}(N_x - N_y)\sin^2\theta\right)(\omega^2 - \omega_0^2), \quad (19)$$

$$Z_2 \approx \gamma_e\csc\theta\left(H_{\rm ext}\sin^2\theta + \frac{M_S}{\mu_0}(N_x - N_y)\sin^2\theta\right)\sigma\omega \quad (20)$$

and then we express the $V_{\rm dc}$ signal as

$$V_{\rm dc} = {\rm A}\sin^2\theta\frac{1}{\left(\omega^2-\omega_0^2\right)^2+\omega^2\sigma^2} \times\left[\cos(\psi)\left(\omega^2-\omega_0^2\right) - \sin(\psi)\sigma\omega\right], \quad (21)$$

where

$$A \equiv \frac{\eta}{4}\Gamma^{-1/2}\gamma_e^2 I H_{\rm Oe}\Delta R\left(H_{\rm ext} + \frac{M_S}{\mu_0}(N_x - N_y)\right). \quad (22)$$

B. Magnetoresistance of the SVGMR strip

In our setup, the magnetoresistance has been measured in the −4 to 4 kOe field range. Figure 4(a) shows relative changes of the resistance under a sweeping field at $\theta = 0^\circ$ (along the exchange bias direction) and $\theta = 90^\circ$ (perpendicular to the exchange bias direction), while in the Fig. 4(b) the same loops are shown in the low field range. It should be emphasized that in our sample the antiparallel state between FL and RL magnetizations has been fixed by the exchange bias field for values up to 1 kOe. The angular dependence of the magnetoresistance [Fig. 4(c)] has been measured in a rotating magnetic field of 100 Oe. The amplitude for each angle has been calculated as the difference between the maximum and minimum values of the spin diode dc voltage from the

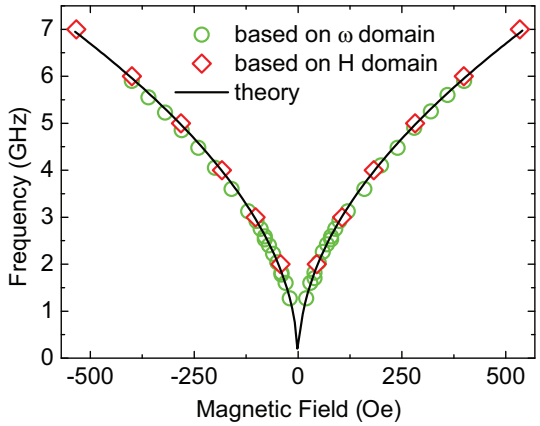

FIG. 5. (Color online) Dispersion relation of the FL magnetization for the SVGMR strip. The H domain denotes a measurement conducted under a sweeping magnetic field at a constant frequency, while the ω domain denotes a measurement conducted in a constant magnetic field with the frequency being swept.

measured spectrum. It remains proportional to $\sin^2(\theta)$, which is in accord with Eq. (21).

C. Dynamics of the SVGMR strip

The FMR induced by the spin diode effect has been investigated as a function of frequency and magnetic field (in the range from −500 to 500 Oe) as shown in Figs. 5 and 6(a). This measurement was performed at $\theta = 90^\circ$, where the amplitude of the FMR signal was maximal [Fig. 4(c)]. The resonance frequency shifts to higher values and the amplitude of the FMR signal decreases as the magnitude of the external magnetic field is increased (Figs. 5 and 6). This behavior is in agreement with theoretical predictions [see Eqs. (18) and (21)]. The theoretical dispersion relation (18) fits the experimental FMR data (Fig. 5) for values derived from VSM measurements (with a saturation magnetization of the FL of 1.03 T and uniaxial anisotropy energy of 0.8 kJ/m^3). The demagnetizing factors $N_x = 0.001\,87$, $N_y = 0.000\,065$, and $N_z = 0.998$ have been calculated with the use of analytical expressions for uniformly magnetized thin films [43], taking into account the nonuniform (composite) character of the FL (1-nm-thick $Co_{90}Fe_{10}$ and 5-nm-thick $Ni_{81}Fe_{19}$).

In order to determine the damping factor α, the dc voltage signal has been measured as a function of field for several frequencies [Fig. 6(a)]. The linear dependence of ΔH as a function of frequency is shown in Fig. 6(b). The damping factor has been determined by fitting a linear function to the measured data using the following equation:

$$\Delta H = \Delta H_0 + \alpha \frac{2\pi f}{\gamma_e}, \tag{23}$$

where ΔH_0 is the frequency-independent component of linewidth broadening that originates from magnetic inhomogeneities. The damping coefficient at $\theta = 90^\circ$ calculated in this way is equal to 0.024.

Finally, we have measured the V_{dc} signal in the frequency domain. The spectra measured at different values of θ are presented in Fig. 7. Figure 7(a) shows the frequency of FMR

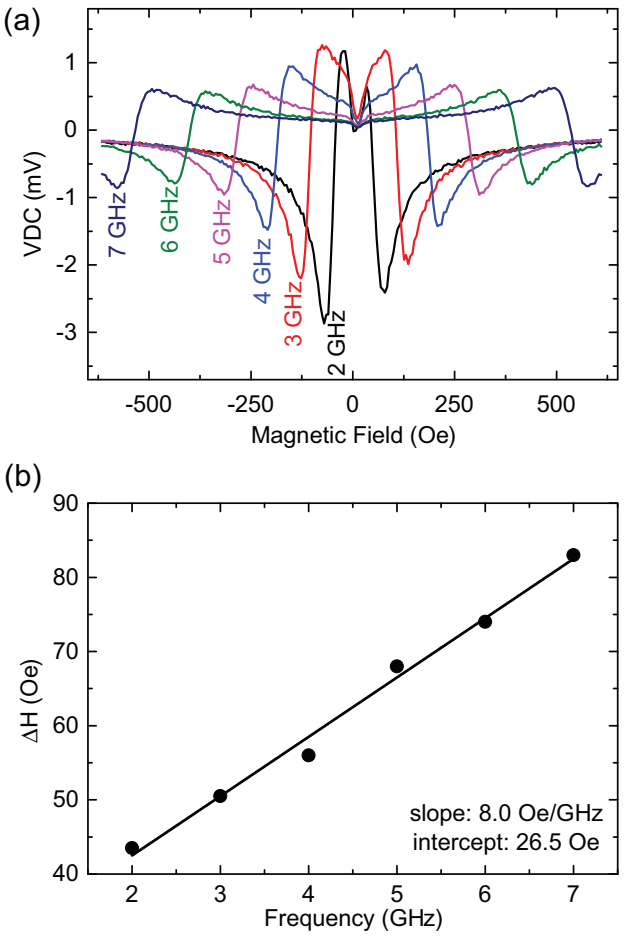

FIG. 6. (Color online) (a) The dc voltage from the spin diode effect as a function of the magnetic field for various frequencies at $\theta = 90^\circ$ and (b) the full width at half maximum ΔH as a function of frequency.

spectra in the full range of rotating angles from 0° to 360°. At θ equal to 0° and 180° the FMR signal disappears, whereas at θ equal to 90° and 270° the signal achieves the maximum value. The exact shapes of the experimental spectral lines are shown in Fig. 7(b). During the rotation of the magnetic field they retain their antisymmetrical character and their amplitudes follow a $\sin^2$ dependence. Moreover, the resonance frequencies do not depend on the direction of the external field and the minima of the antisymmetrical curves have greater absolute values than their maxima.

In Fig. 7(c) we depict V_{dc} curves plotted from Eq. (21) with the phase shift ψ set to zero so that they are purely antisymmetrical, similarly to the experiment. One can see that all the features of experimental spectra mentioned above are reproduced.

D. Comparison of spin diode efficiency in GMR and permalloy strips

A similar experiment has also been conducted on permalloy strips. A 20-nm-thick $Ni_{80}Fe_{20}$ layer has been deposited on an oxidized silicon wafer by magnetron sputtering. Using electron-beam lithography and lift-off method, permalloy

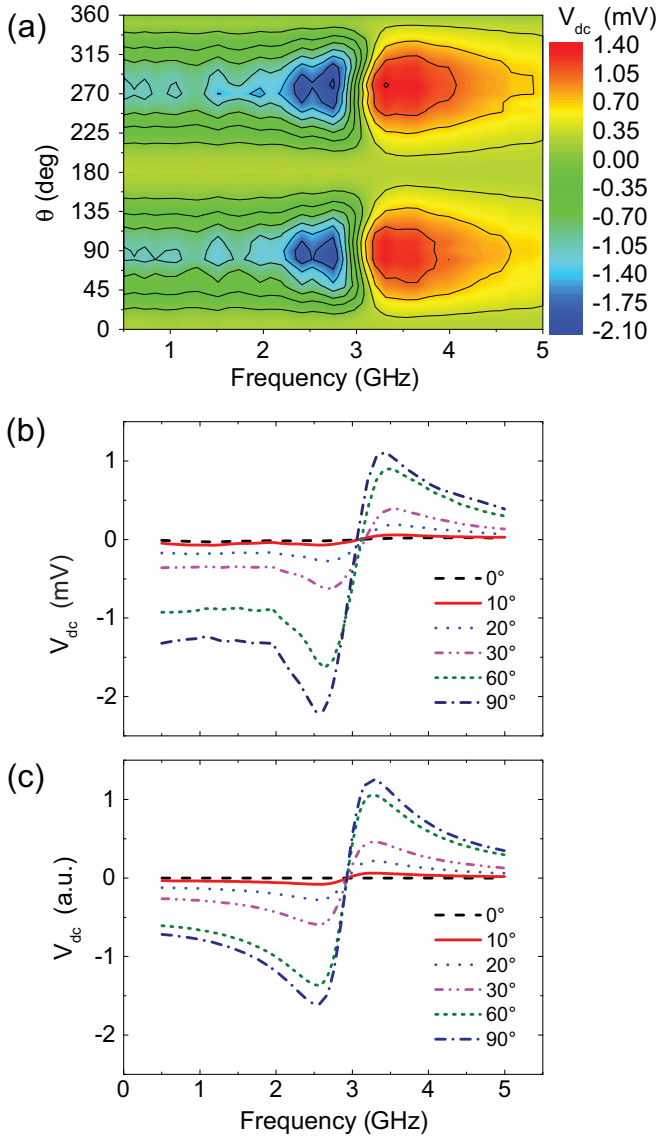

FIG. 7. (Color online) (a) The dc voltage originating from the spin diode effect as a function of the magnetic field angle θ and (b) frequency. (c) Theoretical spectra predicted by Eq. (21).

strips of dimensions similar to those of the SVGMR samples discussed above were fabricated. We found that, although the FMR signal still could be measured in this case, its amplitude was significantly smaller. The strip resistance was about two times larger (346 Ω) and the magnetoresistance was an order

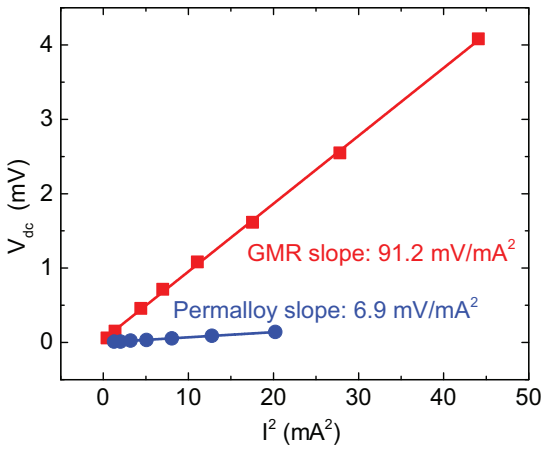

FIG. 8. (Color online) Efficiency of the spin diode effect in SVGMR and permalloy strips.

of magnitude smaller than in the case of the SVGMR strip. The comparison between efficiencies of the spin diode effect for both types of sample shows that the efficiency in the SVGMR strip is several times larger than in the permalloy one, as shown in Fig. 8. This is consistent with previous reports on detection sensitivity being significantly larger in SVGMR strips than in commonly used AMR devices [4,29].

V. CONCLUSION

The spin diode effect was investigated both theoretically and experimentally in GMR strips. Measurements of both static magnetoresistance and the magnetization dynamics have been performed. In the GMR multilayer system, the symmetry of the current distribution is broken and a noncompensated Oersted field appears in the FL, which enables the V_{dc} signal generation upon microwave injection. The measured amplitude of the V_{dc} signal has been shown to be significantly stronger than in commonly used AMR-based NiFe devices. We have provided a comprehensive theoretical model for calculations of the spin diode signal and used it to obtain V_{dc} as a function of frequency, external magnetic field, and angle at which the field is applied. The theoretical results are in good quantitative agreement with the experimental data.

ACKNOWLEDGMENTS

We acknowledge the Polish National Science Center Grant No. DEC-2012/04/M/ST7/00799. Numerical calculations were supported in part by the PL-GRID infrastructure. W.S. acknowledges the Foundation for Polish Science scholarship under START Programme.

[1] O. Prokopenko, I. Krivorotov, T. Meitzler, E. Bankowski, V. Tiberkevich, and A. Slavin, in *Magnonics: From Fundamentals to Applications*, edited by S. O. Demokritov and A. N. Slavin, Topics in Applied Physics Vol. 125 (Springer, Berlin, 2013), p. 143.

[2] J.-V. Kim, Solid State Phys. **63**, 217 (2012).

[3] K. Sattler, *Handbook of Nanophysics: Functional Nanomaterials* (CRC, Boca Raton, 2010).

[4] A. Yamaguchi, H. Miyajima, T. Ono, Y. Suzuki, S. Yuasa, A. Tulapurkar, and Y. Nakatani, Appl. Phys. Lett. **90**, 182507 (2007).

[5] M. Harder, Z. X. Cao, Y. S. Gui, X. L. Fan, and C.-M. Hu, Phys. Rev. B **84**, 054423 (2011).

[6] N. Mecking, Y. S. Gui, and C.-M. Hu, Phys. Rev. B **76**, 224430 (2007).

[7] H. Kurebayashi, J. Sinova, D. Fang, A. C. Irvine, T. D. Skinner, J. Wunderlich, V. Novák, R. P. Campion, B. L. Gallagher, E. K. Vehstedt *et al.*, Nat. Nanotech. **9**, 211 (2014).

[8] A. Tulapurkar, Y. Suzuki, A. Fukushima, H. Kubota, H. Maehara, K. Tsunekawa, D. Djayaprawira, N. Watanabe, and S. Yuasa, Nature (London) **438**, 339 (2005).

[9] J. C. Sankey, P. M. Braganca, A. G. F. Garcia, I. N. Krivorotov, R. A. Buhrman, and D. C. Ralph, Phys. Rev. Lett. **96**, 227601 (2006).

[10] J. Sankey, Y.-T. Cui, J. Sun, J. Slonczewski, R. Buhrman, and D. Ralph, Nat. Phys. **4**, 67 (2007).

[11] W. Skowroński, M. Czapkiewicz, M. Frankowski, J. Wrona, T. Stobiecki, G. Reiss, K. Chalapat, G. S. Paraoanu, and S. van Dijken, Phys. Rev. B **87**, 094419 (2013).

[12] W. Skowroński, M. Frankowski, J. Wrona, T. Stobiecki, P. Ogrodnik, and J. Barnaś, Appl. Phys. Lett. **105**, 072409 (2014).

[13] H. Kubota, A. Fukushima, K. Yakushiji, T. Nagahama, S. Yuasa, K. Ando, H. Maehara, Y. Nagamine, K. Tsunekawa, D. Djayaprawira *et al.*, Nat. Phys. **4**, 37 (2007).

[14] Y. S. Gui, S. Holland, N. Mecking, and C.-M. Hu, Phys. Rev. Lett. **95**, 056807 (2005).

[15] M. Costache, S. Watts, M. Sladkov, C. Van der Wal, and B. Van Wees, Appl. Phys. Lett. **89**, 232115 (2006).

[16] Y. S. Gui, N. Mecking, X. Zhou, G. Williams, and C.-M. Hu, Phys. Rev. Lett. **98**, 107602 (2007).

[17] X. Hui, A. Wirthmann, Y. Gui, Y. Tian, X. Jin, Z. Chen, S. Shen, and C.-M. Hu, Appl. Phys. Lett. **93**, 232502 (2008).

[18] S. Goennenwein, S. Schink, A. Brandlmaier, A. Boger, M. Opel, R. Gross, R. Keizer, T. Klapwijk, A. Gupta, H. Huebl *et al.*, Appl. Phys. Lett. **90**, 162507 (2007).

[19] A. Wirthmann, X. Hui, N. Mecking, Y. Gui, T. Chakraborty, C.-M. Hu, M. Reinwald, C. Schüller, and W. Wegscheider, Appl. Phys. Lett. **92**, 232106 (2008).

[20] M. V. Costache, M. Sladkov, S. M. Watts, C. H. van der Wal, and B. J. van Wees, Phys. Rev. Lett. **97**, 216603 (2006).

[21] E. Saitoh, M. Ueda, H. Miyajima, and G. Tatara, Appl. Phys. Lett. **88**, 182509 (2006).

[22] O. Mosendz, J. E. Pearson, F. Y. Fradin, G. E. W. Bauer, S. D. Bader, and A. Hoffmann, Phys. Rev. Lett. **104**, 046601 (2010).

[23] O. Mosendz, V. Vlaminck, J. E. Pearson, F. Y. Fradin, G. E. W. Bauer, S. D. Bader, and A. Hoffmann, Phys. Rev. B **82**, 214403 (2010).

[24] P. Saraiva, A. Nogaret, J. C. Portal, H. E. Beere, and D. A. Ritchie, Phys. Rev. B **82**, 224417 (2010).

[25] Y. Kajiwara, K. Harii, S. Takahashi, J. Ohe, K. Uchida, M. Mizuguchi, H. Umezawa, H. Kawai, K. Ando, K. Takanashi *et al.*, Nature (London) **464**, 262 (2010).

[26] C. Sandweg, Y. Kajiwara, K. Ando, E. Saitoh, and B. Hillebrands, Appl. Phys. Lett. **97**, 252504 (2010).

[27] L. Liu, T. Moriyama, D. C. Ralph, and R. A. Buhrman, Phys. Rev. Lett. **106**, 036601 (2011).

[28] A. Azevedo, L. H. Vilela-Leão, R. L. Rodríguez-Suárez, A. F. Lacerda Santos, and S. M. Rezende, Phys. Rev. B **83**, 144402 (2011).

[29] J. Kleinlein, B. Ocker, and G. Schmidt, Appl. Phys. Lett. **104**, 153507 (2014).

[30] T. Nozaki, Y. Shiota, S. Miwa, S. Murakami, F. Bonell, S. Ishibashi, H. Kubota, K. Yakushiji, T. Saruya, A. Fukushima *et al.*, Nat. Phys. **8**, 491 (2012).

[31] A. Thiaville and Y. Nakatani, J. Appl. Phys. **104**, 093701 (2008).

[32] D. Griffiths, *Introduction to Electrodynamics* (Pearson, Upper Saddle River, 2013).

[33] E. Weisstein, *MathWorld: The Web's Most Extensive Mathematics Resource* (Wolfram Research, Champaign, 2004), http://mathworld.wolfram.com/SphericalCoordinates.html.

[34] B. Dieny, V. S. Speriosu, S. S. P. Parkin, B. A. Gurney, D. R. Wilhoit, and D. Mauri, Phys. Rev. B **43**, 1297(R) (1991).

[35] S. Parkin, Z. Li, and D. J. Smith, Appl. Phys. Lett. **58**, 2710 (1991).

[36] M. J. Donahue and D. G. Porter, National Institute of Standards and Technology Report No. 6376, 1999 (unpublished), p. 158.

[37] E. Sondheimer, Adv. Phys. **1**, 1 (1952).

[38] P. Desai, T. Chu, H. James, and C. Ho, J. Phys. Chem. Ref. Data **13**, 1069 (1984).

[39] K. Eid, W. Pratt, Jr., and J. Bass, J. Appl. Phys. **93**, 3445 (2003).

[40] K. Eid, R. Fonck, M. Darwish, W. Pratt, Jr., and J. Bass, J. Appl. Phys. **91**, 8102 (2002).

[41] H. Yuasa, M. Yoshikawa, Y. Kamiguchi, H. Iwasaki, M. Takagishi, M. Sahashi *et al.*, J. Appl. Phys. **92**, 2646 (2002).

[42] N. Strelkov, A. Vedyaev, and B. Dieny, J. Appl. Phys. **94**, 3278 (2003).

[43] A. Aharoni, J. Appl. Phys. **83**, 3432 (1998).